Soils and Foundations 2014;54(5):955–966

HOSTED BY

ELSEVIER

CrossMark

The Japanese Geotechnical Society

Soils and Foundations

www.sciencedirect.com

journal homepage: www.elsevier.com/locate/sandf

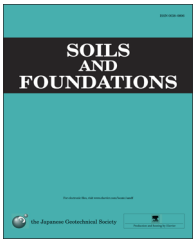

Static liquefaction-triggering analysis considering soil dilatancy

Abouzar Sadrekarimi*

Western University, Department of Civil and Environmental Engineering, 3010D Spencer Engineering Building, London, Ont., Canada N6A 5B9

Received 12 November 2013; received in revised form 9 May 2014; accepted 12 June 2014
Available online 12 October 2014

Abstract

The failure of a sloping ground due to static liquefaction occurs when the shear stress applied by a monotonic triggering load exceeds the undrained yield (peak) shear strength of the saturated liquefiable cohesionless soil. Current practices for determining the in-situ undrained yield strength for grounds subjected to static shear stress rely on either a suite of costly laboratory tests on undisturbed field samples or empirical correlations based on in-situ penetration tests, which fail to account for the effect of soil dilatancy in decreasing the degree of strain-softening and the brittleness of cohesionless soils with an increasing penetration resistance. In this study, the effect of soil dilatancy on the static liquefaction failure of cohesionless soils is characterized by an empirical relationship between the soil brittleness index and the undrained yield strength from a database of 813 laboratory shear tests collected from the past literature. The application of this relationship for estimating the static liquefaction-triggering strength of cohesionless soils under sloping ground conditions is validated by comparing several cases of liquefaction flow failures. Finally, a procedure is briefly demonstrated for evaluating the triggering of static liquefaction in a dyke to the north of Wachusett Dam and Duncan Dam which incorporates the dilatancy behavior of cohesionless soils in a semi-empirical procedure based on in-situ penetration tests.

Keywords: In-situ testing; Laboratory tests; Liquefaction; Sands; Shear strength

1. Introduction

Failure due to liquefaction flows occurs in saturated loose cohesionless soils subjected to an initial static shear stress (e.g., in a sloping ground or beneath a foundation) when the soil resistance becomes lower than the static driving shear stress. The sudden nature and the very large shear displacements associated with liquefaction flow failures have made this phenomenon one of the most catastrophic mechanisms in the failure of slopes and embankments of saturated loose cohesionless soils. A liquefaction flow failure requires a triggering mechanism to initiate liquefaction and undrained strain-softening.

When a soil is sheared, its volume may increase (dilate) or decrease (contract) depending on its density and the magnitude of the effective stress applied on the soil. However, when this change in volume is inhibited during undrained (constant-volume) shearing, the tendency to dilate ("positive dilatancy") or contract ("negative dilatancy") is offset by an equally opposite elastic volumetric strain, which produces changes in the pore water pressure (Jefferies and Been, 2006). As illustrated in Fig. 1, static liquefaction is triggered in a saturated loose cohesionless soil by a monotonically-increasing shear load (e.g., raising the embankment height, oversteepening, the slope, toe erosion, rapid sediment accumulation, construction loading, weight of the construction/repair equipment, tidal changes, reservoir filling, slumping and progressive

*Tel.: +1 519 661 2111 x80334.
E-mail address: asadrek@uwo.ca
Peer review under responsibility of The Japanese Geotechnical Society.

http://dx.doi.org/10.1016/j.sandf.2014.09.009

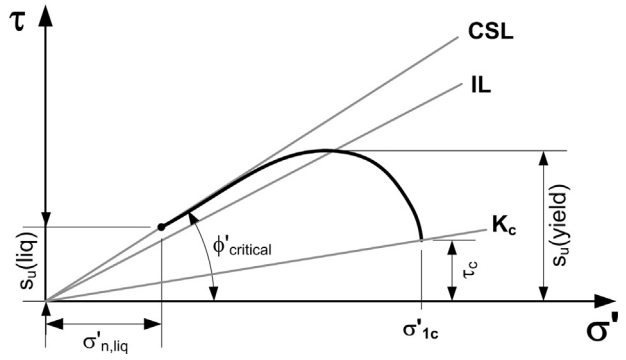

Fig. 1. Schematic liquefaction-triggering mechanism by monotonic undrained stress path.

failure leading to steeper slopes) when the undrained effective stress path crosses the instability line (Lade, 1992) at s_u(yield). Strain-softening subsequently follows the initiation of liquefaction until a reduced post-liquefaction strength, s_u(liq), is mobilized at large shear strains (Terzaghi et al., 1996). The February 1994 flowslide failure of the Merriespruit gold mine tailings dam in Virginia, South Africa, which released 600,000 m^3 of waste tailings over a distance of more than 2000 m, killed 17 people and destroyed 280 houses (Fourie et al., 2001), and the March 1918 flowslide failure of Calaveras Dam in California, which traveled about 200 m (Hazen, 1918), are examples of liquefaction flow failures triggered by monotonic loads produced by the oversteepening of the Merriespruit tailings dam and the rapid construction of the Calaveras Dam. Liquefaction flow failures resulting from monotonically-increasing loads have also occurred extensively in natural soil deposits in offshore or coastal areas, for example, along the shores of the straits between the islands of Zeeland, Netherlands (Bjerrum, 1971; Koppejan et al., 1948) or along the banks of the Mississippi River (Castro, 1969) damaging dykes and revetments and flooding downstream lands. Olson (2001) and Muhammad (2012) described several other cases of liquefaction flow failures. Understanding and quantifying the fundamental soil behavior associated with the triggering of these tragic events is an important step in liquefaction analysis and in determining the risk of liquefaction flow failures. This is particularly necessary for the design of large and high-risk earth structures, such as mine tailing impoundments, earth dams, and heavy building foundations for which a liquefaction failure has the potential to result in a flowslides, extensive damage, and loss of lives. Proper liquefaction mitigation and soil improvement techniques could then be implemented in the design or retrofitting of these critical structures if liquefaction triggering is found. Dilatancy is a fundamental aspect of soil shearing behavior which depends on soil density and the effective stress level. Based on a large database of laboratory shear tests, this study introduces an empirical relationship between s_u(yield) and s_u(liq), which captures the effect of soil dilatancy on the undrained strength of loose cohesionless soils. This relationship is employed for the estimation of s_u(yield) from in-situ penetration tests.

2. Liquefaction-triggering analysis of sloping grounds

An analysis of liquefaction triggering can determine whether or not liquefaction and a loss in undrained strength would occur in a liquefiable cohesionless soil under given loading conditions. This involves evaluating whether the combined initial static (τ_c) and monotonic-triggering shear stresses are sufficient to overcome s_u(yield). Several methods are available for determining the s_u(yield) of cohesionless soils. These include: (A) laboratory shear tests, (B) numerical analyses of soil constitutive models (Buscarnera and Whittle, 2013; Fuentes et al., 2012; Jefferies, 1993; Mroz et al., 2003; Park and Byrne, 2004), and (C) empirical correlations with in-situ penetration tests (Mesri, 2007; Olson and Stark, 2002; Stark and Mesri, 1992). Some of the major challenges and practical limitations of these methods are described in the following paragraphs.

Laboratory shear tests (Method A) provide the only direct measurement of s_u(yield). However, as the s_u(yield) of cohesionless soils is highly sensitive to the soil composition (mineralogy and gradation), fabric, sample disturbance, and soil-mixing effects, undisturbed samples obtained by ground freezing techniques should be used. While ground freezing is the only sampling method that can preserve the in-situ microstructure of cohesionless soils and provide relatively undisturbed samples (Hofmann et al., 2000), it is an expensive and onerous procedure that is only feasible in certain large projects. Even then, the s_u(yield) measured by subjecting a limited number of undisturbed samples to a particular mode of shear (e.g., triaxial compression, triaxial extension or direct simple shear) will not represent the in-situ liquefaction-triggering behavior of the entire soil layer. This is because of the natural heterogeneity and variability of in-situ cohesionless soils and the complex loading conditions present in the field. On the other hand, although numerical analyses (e.g., finite element or finite difference analyses) with advanced soil constitutive models (Method B) can replicate a wide range of loading conditions, it is difficult to apply or validate such analyses even with the best-documented cases. This is because of the difficulties and uncertainties involved with the selection and calibration of the soil constitutive model, the complex input parameters, and the loading conditions. A number of advanced laboratory shear tests on undisturbed soil samples would be required to obtain the calibration parameters for the soil constitutive model, compromising the feasibility of this method for routine liquefaction-triggering analyses.

Accordingly, empirical correlations with the in-situ Standard Penetration Test (SPT) blow count, $(N_1)_{60}$, or Cone Penetration Test (CPT) tip resistance, q_{c1} (Method C), are often used for estimating the in-situ triggering strength because of their simplicity, convenience, lower costs, and nearly continuous measurements. These correlations, which were established based on past liquefaction flow failures (Mesri, 2007; Olson and Stark, 2003; Stark and Mesri, 1992), fall short of accounting for the fundamental effect of a soil's dilatancy potential to decrease the amount of loss in undrained strength following the triggering of static liquefaction with increasing penetration resistance.

Fig. 2 presents the stress-strain shearing behaviors of Illinois River sand (Sadrekarimi, 2009) and Toyoura sand (Verdugo, 1992) specimens at different consolidation relative densities (D_{rc}) in undrained triaxial compression tests isotropically consolidated to confining stresses of 370 kPa and 490 kPa, respectively. According to this figure, while s_u(yield) and s_u(liq) both increase with an increasing D_{rc}, s_u(liq) exhibits larger increments with an increasing D_{rc} than s_u(yield), such that the amount of strength reduction from s_u(yield) to s_u(liq) decreases with the increasing soil dilatancy potential as a result of the increasing D_{rc}. As the normalized in-situ penetration resistance ($(N_1)_{60}$ or q_{c1}) is essentially a measure of D_{rc} (Cubrinovski and Ishihara, 1999; Jamiolkowski et al., 1985; Kulhawy and Mayne, 1990), the amount of strength reduction from s_u(yield) to s_u(liq) would also decrease with an increasing $(N_1)_{60}$ or q_{c1} as a result of the increased dilatancy potential.

However, as illustrated in Fig. 3, none of the existing empirical relationships (Mesri, 2007; Olson and Stark, 2002, 2003; Stark and Mesri, 1992) account for this fundamental soil behavior. These methods assume that s_u(yield) increases with an increasing $(N_1)_{60}$ or q_{c1} at the same rate (Mesri, 2007; Olson and Stark, 2002, 2003) or at an even greater rate (Stark and Mesri, 1992) than s_u(liq). Hence, the loss in the soil's undrained strength from s_u(yield) to s_u(liq) remains the same or increases with an increasing $(N_1)_{60}$ or q_{c1}, whereas these two lines should meet at a certain penetration resistance when the soil strain-softening behavior diminishes. A direct implication of this negligence is that these correlations cannot differentiate among liquefaction flow failures with different travel distances, and therefore, cannot explain, for example, why the liquefaction flow failure of the Merriespruit tailings dam traveled more than 2000 m, while the flow failure of the Calaveras Dam moved about 200 m. In summary, the existing methods for liquefaction-triggering analyses and the estimation of s_u(yield) for grounds subject to static shear stress require either advanced and costly laboratory shear tests or are incompatible with the dilatancy behavior of cohesionless soils. These could result in considerable expenses or inaccuracies in the estimations of s_u(yield).

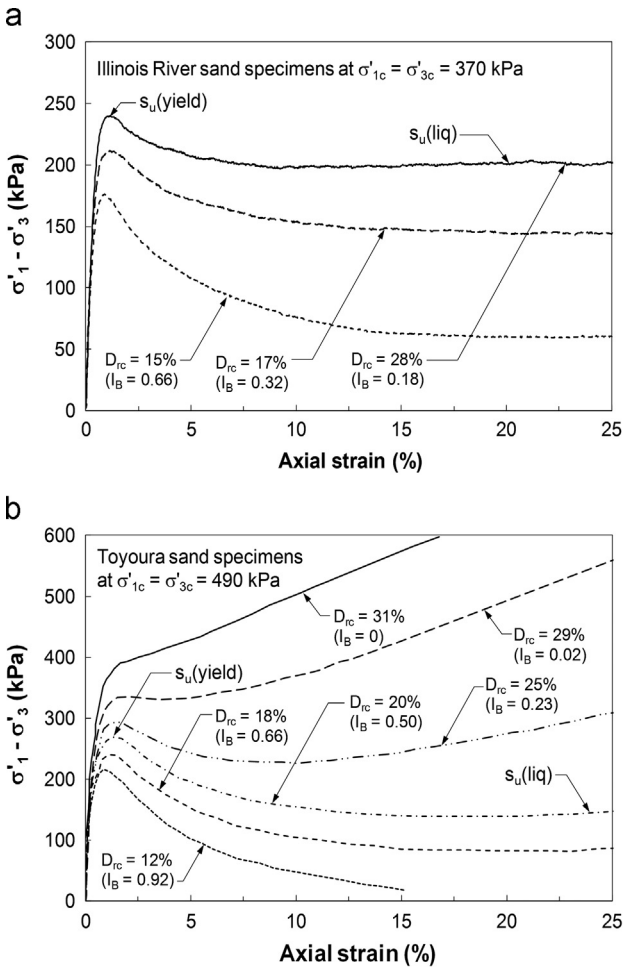

Fig. 2. Undrained shear behavior of (a) Illinois River sand (Sadrekarimi, 2009) and (b) Toyoura sand (Verdugo, 1992) specimens in triaxial compression tests at different relative densities.

3. Database of laboratory shear tests

A large database of 813 direct simple shear (DSS) tests, hollow cylindrical torsional shear (HCTS) tests, plane strain compression shear (PSC) tests, ring shear (RS) tests, and axisymmetric triaxial compression shear (TxC) tests are collected in this study. They cover a very wide range of fines contents, FC (0–84.6%), consolidation relative densities, D_{rc} (−41 to 94% corresponding to consolidation void ratios of e_c=0.34–1.287), consolidation major principal stresses, σ'_{1c} (29–8939 kPa), specimen preparation techniques (AP: air pluviation; WP: water pluviation; MT: moist tamping), and consolidation principal stress ratios ($K_c=\sigma'_{3c}/\sigma'_{1c}$) ranging from 0.33 to 1.0. Table 1 summarizes these experiments and their specimen preparation methods. Since the dominant mode of shear within the zone of liquefaction for most of the past liquefaction flow failures is similar to triaxial compression and simple shearing conditions (Olson and Stark, 2003), only these modes of shearing are considered in this paper. For DSS and RS tests, the application of σ'_{1c} and consolidation occurs under a laterally constrained condition imposed by the rigid lateral boundaries of these apparatuses. As a result, K_c corresponding to a laterally constrained condition (K_o) is produced in these tests.

As shown in Figs. 1 and 2, s_u(yield) and s_u(liq) describe the liquefaction-triggering condition and the subsequent behavior after liquefaction occurs, respectively. The normalized difference between s_u(yield) and s_u(liq) is used in this study to quantify the amount of undrained shear strength reduction which occurs following the initiation of liquefaction. This is commonly defined by the undrained brittleness index, I_B, as shown below (Bishop, 1971):

$$I_B = \frac{s_u(\text{yield}) - s_u(\text{liq})}{s_u(\text{yield})} \quad (1)$$

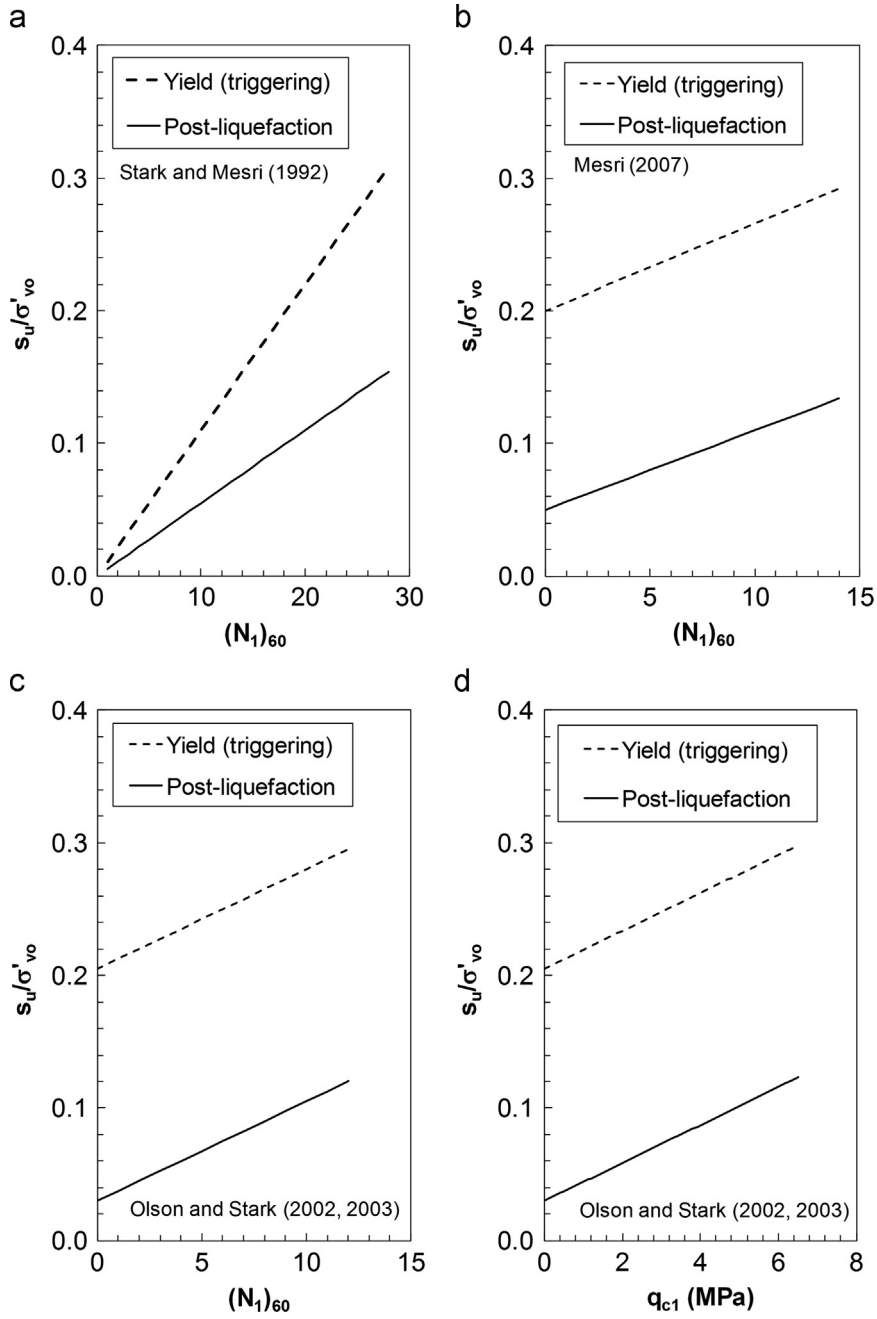

Fig. 3. Existing empirical correlations of s_u(yield)/σ'_{vo} and s_u(liq)/σ'_{vo} with in-situ penetration tests (Stark and Mesri, 1992; Olson and Stark, 2002, 2003; Mesri, 2007).

I_B lies in the range of from 0 to 1, where $I_B=1$ indicates a very brittle soil behavior associated with an extremely low s_u(liq), while $I_B=0$ occurs in non-brittle or strain-hardening soils where no strength reduction occurs during undrained shear. In the following section, the liquefaction behavior of cohesionless soils is characterized in terms of I_B for the 813 laboratory shear tests shown in Table 1. Note that s_u(yield) includes any initial shear stress (τ_c), resulting from anisotropic consolidation, and the additional shear stress required to cause strain-softening and liquefaction. The post-liquefaction undrained strength, s_u(liq), is selected at the end of the tests where a critical state of constant effective stress and shear stress is attained following strain-softening behavior. However, some of the undrained triaxial shear tests exhibited a brief strain-hardening towards the end of the tests after an extended range of constant effective stress and shear stress. In these cases, the minimum undrained strength following strain-softening behavior, which is more relevant to flow failures and stability analyses (Ishihara, 1993; Yoshimine et al., 1999), is adopted as s_u(liq). This is because when instability and deformation occur in the field, the soil behavior may become dynamic and turbulent due to inertial effects, and hardening may not be possible under such circumstances.

Table 1
Summary of laboratory shear tests used in this study.

Shear test (# of tests)	Sand[a]	K_c	FC (%)	Reference
DSS (13)	Monterey #0 (MT)	K_o	0	Riemer (1992)
	Ottawa (AP)		0	Sivathayalan and Ha (2011)
HCTS (119)	Babolsar (MT)	0.33–1.0	0	Keyhani and Haeri (2013)
	Fraser River (WP)	0.5–1.0	0	Sivathayalan and Vaid (2002)
	Ottawa 20-30 (AP)	1.0	0	Alarcon-Guzman et al. (1988)
	Syncrude (MT)	1.0	12	Wride and Robertson (1997a)
	Toyoura (AP)	0.5–1.0	0	Yoshimine et al. (1998, 1999)
PSC (43)	Changi (MT)	0.4–0.5	0.4	Chu and Wanatowski (2009), Wanatowski (2007), Wanatowski and Chu (2007)
	Masonry (MT)	0.4–0.5	0	Harris (1994), Mooney (1996)
	Ottawa (MT)	0.5	0	Harris (1994)
RS (64)	Illinois River (MT)	K_o	1	Sadrekarimi (2009)
	Mississippi River (AP)		38	
	Ottawa (MT)		0	
	M10 (MT)		76.2	Wang (1999b)
	M20 (MT)		78.2	
	M30(MT)		80.4	
	M50 (MT)		84.6	
	S7 sand (MT)		10	
	S8 sand (MT)		73.9	
	Osaka group sand (AP)		1	Wang (1999a)
	Silica sand (AP)		5	
	Toyoura (AP)		1	
TxC (574)	Alaskan (MT)	1.0	5	Jefferies and Been (2006)
	Amauligak F-24 (MT)	1.0	21	
	Banding sand (MT)	0.5–1.0	0	Castro et al. (1982), Jefferies and Been (2006)
	Barco 71 (MT)	1.0	0	Omar (2013)
	Changi (MT)	0.43–1.0	0.4	Wanatowski and Chu (2007)
	Coal mine tailings (MT)	1.0	0–4	Dawson et al. (1998)
	Duval copper tailings (MT)	1.0	37	Chen (1984)
	Erksak (MT)	1.0	0.7–1.0	Been et al. (1991), Jefferies and Been (2006)
	Fraser River (MT, WP)	0.49–1.0	2–3	Konrad and Pouliot (1997), Vaid et al. (2001), Wride and Robertson (1997b)
	Garnet tailings (MT)	0.5–1.0	0–20	Highter and Tobin (1980), Lavigne (1988)
	Hostun RF (MT)	0.36–1.0	0	Di Prisco et al. (1995), Doanh et al. (1997), Finge et al. (2006), Gajo and Piffer (1999), Konrad (1993)
	Illinois River (MT)	1.0	1	Sadrekarimi (2009)
	Leighton Buzzard (MT)	1.0	0	Hird and Hassona (1990), Sladen et al. (1985)
	M31 sand (WP)	1.0	0	Tsomokos and Georgiannou (2010)
	Merriespruit tailings (MT)	0.54–1.0	0–60	Fourie and Tshabalala (2005)
	Mississippi River (AP)	1.0	38	Sadrekarimi (2009)
	Monterey #0 (MT)	0.5–1.0	0	Riemer (1992)
	Nerlerk sand (MT)	1.0	0–12	Hird and Hassona (1990), Jefferies and Been (2006), Sladen et al. (1985)
	Ottawa banding (MT)	1.0	2	Dennis (1988)
	Ottawa 20/40 (MT)	1.0	0	Sadrekarimi (2009)
	Ottawa sand with fines (MT)	1.0	0–15	Murthy et al. (2007)
	Ottawa C109 with Kaolinite (MT)	1.0	0, 5	Sasitharan (1994)
	Ottawa sand with Kaolinite (MT)	1.0	5–20	Skirrow (1996)
	Portaway (MT)	1.0	1	Wang (2005)
	Sacramento River (MT, AP)	0.44–1.0	0	Kramer and Seed (1988), Lee (1965)
	Sand B (MT)	1.0	0	Castro (1969)
	Sand C (MT)	1.0	1	
	Sydney (MT)	1.0	0	Chu (1995)
	Syncrude tailings (MT)	0.5–1.0	10–12	Sladen and Handford (1987), Wride and Robertson (1997a)
	Ticino (MT)	1.0	0	Konrad (1993)
	Till Sand (MT)	1.0	32	
	Tottori (MT)	1.0	0	Takeshita et al. (1995)
	Toyoura (AP, MT)	0.33–1.0	0	Kato et al. (2001), Verdugo (1992), Yoshimine (1996)

[a]Letters in parentheses represent specimen preparation methods as AP for air pluviation, MT for moist tamping, and WP for water pluviation.

4. Results and discussions

Fig. 4 presents I_B versus $\sigma'_{1c}/\sigma'_{n,liq}$ for the large database of laboratory shear tests presented in Table 1, where σ'_{1c} and $\sigma'_{n,liq}$ are the major consolidation principal stress and the post-liquefaction (i.e., associated with s_u(liq)) normal stress on the failure plane, respectively. These correspond to the effective vertical stresses in the DSS, HCTS, and RS tests. For the PSC and TxC tests, $\sigma'_{n,liq}$ is calculated on the Coulomb failure plane at an angle of $45+\phi'_{critical}/2$ with respect to the major principal stress plane using the following equation:

$$\sigma'_{n,liq} = \frac{1}{2}\left(\sigma'_{1,liq}+\sigma'_{3,liq}\right) - \frac{1}{2}\left(\sigma'_{1,liq}-\sigma'_{3,liq}\right)\sin\ \phi'_{critical} \quad (2)$$

where $\sigma'_{1,liq}$ and $\sigma'_{3,liq}$ are the major and minor post-liquefaction principal stresses, respectively, and $\phi'_{critical}$ is the critical state friction angle. The ranges in data are curve-fitted by the following equation:

$$I_B = \exp\left(\frac{A}{B-\sigma'_{1c}/\sigma'_{n,liq}} - 0.03\right) \quad (3)$$

Data from all modes of shear are correlated with the average constants of $A=2.1$ and $B=1.5$ with a coefficient of correlation of 0.86. Eq. (3), with constants of $A=1.1$, $B=1.1$, and $A=3.6$, $B=1.9$, encompasses the upper and lower bounds of the data, respectively. Fig. 4 and Eq. (3) indicate that the severity of the liquefaction and the strain-softening increases with an increasing σ'_{1c} or a decreasing $\sigma'_{n,liq}$ for cohesionless soils.

Note that the upper boundary of Eq. (3) (with $A=1.1$ and $B=1.1$) is largely driven by the TxC tests on the moist tamped specimens in Fig. 4d. This is because moist tamping produces a comparatively stiffer sand fabric and moist tamped specimens often exhibit larger magnitudes of s_u(yield); and thus, more severe strain-softening and larger brittleness is ensued compared to specimens prepared by other methods (DeGregorio, 1990; Høeg et al., 2000; Huang et al., 2004; Mulilis et al., 1977). Eq. (3) further implies that strain-softening and brittle behavior ($I_B > 0$) arise for an average $\sigma'_{1c}/\sigma'_{n,liq} > 2.3$, which is very close to the ratio suggested by Ishihara (1993) for the occurrence of strain-softening.

5. Comparison with past static liquefaction flow Failures

The application of Eq. (3) – developed based on a large database of laboratory shear tests – to static liquefaction failures, is evaluated by comparing the s_u(yield) estimated from this equation with those mobilized in several cases of static liquefaction flow failures presented in Table 2. Except for the submarine flowslide in Kitimat, British Columbia, for which s_u(yield) and s_u(liq) are obtained from in-situ vane shear tests (Morrison, 1984), I_B is calculated for these cases based on the s_u(yield) and s_u(liq) back-calculated from static slope stability analyses of the pre- and post-failure slope geometries, respectively (Muhammad, 2012; Olson, 2001). As described by Olson (2001) and Muhammad (2012), s_u(yield) was obtained by back-calculating the shear stress mobilized in the liquefiable soil zones of the pre-failure slope geometry immediately prior to the static flow failure. In these analyses, s_u(yield) within the zone of liquefaction was varied in Spencer's (1967) limit equilibrium slope stability analysis until a factor of safety of one was achieved, while appropriate fully mobilized drained shear strengths were assigned to the soil zones initially above the phreatic surface or to the

Table 2
Static liquefaction flow failures evaluated in this study.

No	Case	Triggering factor	s_u (yield)/σ'_{vo}	s_u (liq)/σ'_{vo}	I_B	Soil type
A	Calaveras dam, USA[a]	Construction loading	0.270 (0.255–0.295)	0.112 (0.093–0.123)	0.584 (0.518–0.684)	Silty sand (FC ≈ 10–50%)
B	Fort Peck dam, USA[a]	Construction loading	0.255 (0.230–0.285)	0.078 (0.048–0.097)	0.695 (0.579–0.832)	Sandy silt (FC ≈ 55%)
C	Helsinki Harbor, Finland[a]	Raising slope height	0.240 (0.210–0.260)	0.060 (0.037–0.098)	0.750 (0.533–0. 858)	Sand
D	Kitimat flowslide, Canada[b]	Disturbance by low tide	0.203	0.017	0.914	Fine silty sand to silt
E	Lake Ackerman road embankment, USA[a]	Weight of construction equipment	0.245 (0.220–0.275)	0.076 (0.066–0.092)	0.690 (0.582–0.760)	Clean sand
F	Sullivan tailings dam, Canada[c]	Raising dam height	0.241 (0.228–0.254)	0.132	0.452 (0.420–0.480)	Hydraulic fill iron tailings
G	Tar Island dyke, Canada[a]	Raising dyke height	0.265 (0.195–0.300)	0.058 (0.037–0.105)	0.781 (0.462–0.460. 875)	Silty sand (FC ≈ 10–30%)
H	Merriespruit tailings dam, South Africa[c]	Oversteepening of slope	0.226 (0.219–0.333)	0.026 (0.004–0.048)	0.885 (0.780–0. 989)	Sandy silt(FC ≈ 60%)
I	Asele road embankment, Sweden[a]	Weight of construction equipment	0.280 (0.232–0.316)	0.104 (0.083–0.125)	0.629 (0.461–0.737)	Silty sand(FC ≈ 23–38%)

[a]Based on limit equilibrium slope stability analyses of Olson (2001).
[b]From in-situ vane shear tests (Morrison, 1984).
[c]Based on limit equilibrium slope stability analyses of Muhammad (2012).

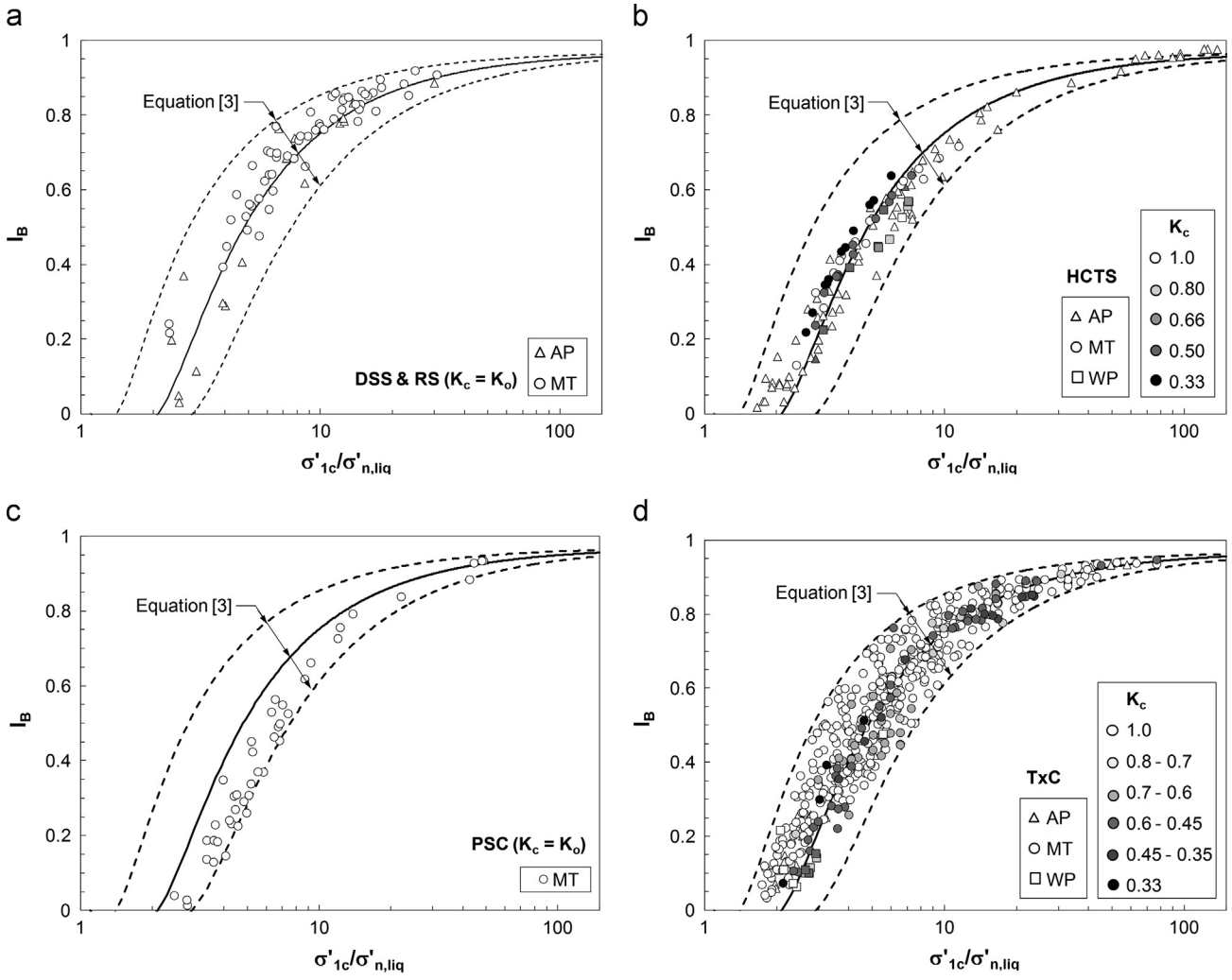

Fig. 4. Variation in I_B with $\sigma'_{1c}/\sigma'_{n,liq}$ for (a) DSS and RS, (b) HCTS, (c) PSC, and (d) TxC shear tests shown in Table 1.

non-liquefied soils. The critical failure surface associated with the minimum back-calculated strength was often found to conform to the descriptions of failure, eyewitness accounts, and the reported post-failure morphology of the failure.

Sufficient information (e.g., postfailure geometry, travel path, and the distance of the failure soil mass) was available in cases A, B, E, and F to consider the kinetics of failure. Therefore, analyses of the kinetics of motion were conducted by Olson (2001) and Muhammad (2012) for these cases based on the procedure described by Davis et al. (1988). In this method, the mobilized shear resistance is initially assumed to be smaller than the static driving shear stress (i.e., weight of the failure mass), causing the accelerated sliding of the failure soil mass. With an increasing downslope displacement and changes in slope geometry, the driving shear stress decreases to an amount smaller than the soil shear resistance, and thereby, decelerating the sliding soil mass until it reaches a full stop (zero velocity) at the end of sliding. The correct s_u(liq) is the shear resistance that provides a kinetically calculated sliding displacement which is reasonably close to the observed travel distance of the failure soil mass. Due to limited information, simplified slope stability analyses (Ishihara et al., 1990) were carried out to estimate s_u(liq) for cases C, G, and I. In these analyses, s_u(liq) was calculated based on the static driving shear stress in the post-failure slope. The ranges in the undrained strengths reported in Table 2 reflect the uncertainties associated with the limits of the liquefied soil zone, the location of the failure surface, and the shear strengths of the non-liquefied soils, as well as the variations in the effects of void redistribution, hydroplaning, mixing with water, and changes in the weight of the liquefied material if the failure mass slid into a body of water (Muhammad, 2012; Olson, 2001).

In order to apply Eq. (3) to the liquefaction flow failures of Tables 2, σ'_{1c} and $\sigma'_{n,liq}$ are replaced, respectively, with the average pre-failure effective vertical stress (σ'_{vo}) and the post-liquefaction effective normal stress on the critical failure plane in the zone of liquefaction. Based on Mohr-Coulomb's failure criterion, the post-liquefaction effective normal stress is further replaced with s_u(liq)/tan($\phi'_{critical}$) in which $\phi'_{critical}$ is the critical state friction angle. Unless laboratory data are available, $\phi'_{critical} = 32^\circ \pm 1^\circ$ is a reasonable assumption for most silica

sands (Andersen and Schjetne, 2012; Bolton, 1986; Sadrekarimi, 2013; Sadrekarimi and Olson, 2011). With these changes, Eqs. (1) and (3) are combined and rearranged as shown below in order to obtain $s_u(\text{yield})/\sigma'_{vo}$ from I_B (in Eq. (4)) or from $s_u(\text{liq})/\sigma'_{vo}$ (in Eq. (5)):

$$\frac{s_u(\text{yield})}{\sigma'_{vo}} = \frac{\tan(32^\circ) \times \ln(I_B+0.03)}{(1-I_B)[B\ln(I_B+0.03)-A]} \quad (4)$$

$$\frac{s_u(yield)}{\sigma'_{vo}} = \frac{s_u(liq)/\sigma'_{vo}}{1.03-\exp\left(\frac{A}{B-\frac{\sigma'_{vo}\tan(32^\circ)}{s_u(\text{liq})}}\right)} \quad (5)$$

Normalization with respect to σ'_{vo} incorporates the variation in σ'_{vo} and allows the comparison of $s_u(\text{yield})$ among field liquefaction failures with different liquefaction depths and Eqs. (4) and (5). According to Fig. 5, the average I_B and $s_u(\text{yield})/\sigma'_{vo}$ of the liquefaction flow failures closely follow the average trend of Eq. (4), indicating that Eq. (4) provides reasonable estimates of $s_u(\text{yield})$ mobilized in the static liquefaction failures of sloping grounds. Note that while the ranges in $s_u(\text{yield})/\sigma'_{vo}$ from Eq. (4) also encompass the $s_u(\text{yield})/\sigma'_{vo}$ variations (error bars) of the liquefaction flow failures, the upper range of Eq. (4) – which is established largely based on TxC shear tests on loose moist tamped specimens (see Fig. 4d) – is significantly larger than the values of $s_u(\text{yield})/\sigma'_{vo}$ from the liquefaction flow failures. This implies that the in-situ fabric of the soils involved in the liquefaction flow failures of Table 2 was likely similar to those developed by air pluviation or water pluviation specimen preparation techniques. Through the combination of Eqs. (4) and (5), the average relationship of $s_u(\text{liq})/\sigma'_{vo}$ with I_B is also presented in Fig. 5. According to this figure, brittleness initially arises primarily by the decrease in $s_u(\text{liq})/\sigma'_{vo}$, while $s_u(\text{yield})/\sigma'_{vo}$ remains roughly around 0.26 for $0.1 < I_B < 0.8$, which reflects the larger impact of D_{rc} (and thus, I_B) on $s_u(\text{liq})/\sigma'_{vo}$ than on $s_u(\text{yield})/\sigma'_{vo}$ (see Fig. 2). However, at $I_B = 0.8$, $s_u(\text{yield})/\sigma'_{vo}$ exhibits a sharp decline and continues to decrease with an increasing I_B at a greater gradient for very brittle

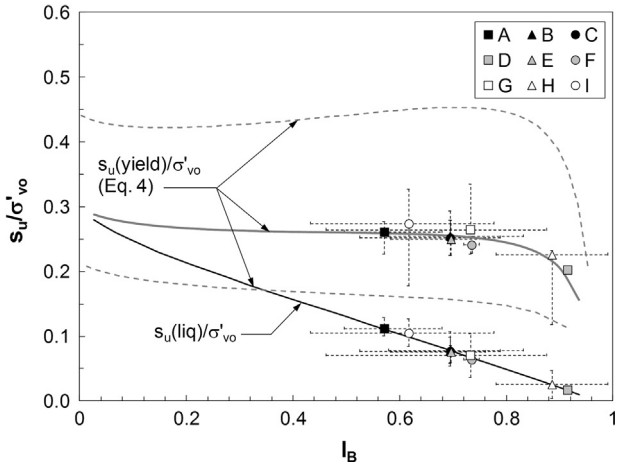

Fig. 5. Comparison of $s_u(\text{yield})/\sigma'_{vo}$ and $s_u(\text{liq})/\sigma'_{vo}$ in liquefaction flow failures shown in Table 2 (datapoints) with Eq. (4).

cohesionless soils ($I_B > 0.8$), which is supported by both laboratory shear tests and field liquefaction flow failures. Although K_c does not appear in Eqs. (3) and (5), based on the plots of Fig. 4, the available soil resistance and the margin of safety against liquefaction triggering at $s_u(\text{yield})$ would decrease with an increasing τ_c beneath a sloping ground or a foundation. Accordingly, a relatively small undrained disturbance (from τ_c to $s_u(\text{yield})$) might initiate a sudden flow failure in a sandy soil under a sloping ground. The risk of such failure increases with an increasing τ_c or slope angle.

Note that void redistribution, pore water pressure migration, water layer formation, particle damage, and strain localization (Kokusho and Kojima, 2002; Kramer and Seed, 1988; Kulasingam et al., 2004; Malvick et al., 2008; Mizanur and Lo, 2012; Sadrekarimi and Olson, 2010a; Sassa, 2000; Seid-Karbasi and Byrne, 2007) would have affected $s_u(\text{yield})$ and $s_u(\text{liq})$ mobilized in field liquefaction flow failures of Table 2, as well as the laboratory shear tests of Table 1 (Ayoubian and Robertson, 1998; Batiste et al., 2004; Boulanger and Truman, 1996; Gilbert and Marcuson, 1988; Sadrekarimi and Olson, 2010a, b; Vaid and Eliadorani, 1998; Wanatowski et al., 2010). The ranges in back-calculated $s_u(\text{yield})/\sigma'_{vo}$ and $s_u(\text{liq})/\sigma'_{vo}$, presented in Fig. 5 and Table 2, ascertain the effects of these phenomena as well as the uncertainties in the shear strength of non-liquefied soils, the location of the failure surface, and the dimensions of the liquefaction zone. Therefore, the combined effects of these phenomena are implicitly accounted for in Figs. 4 and 5 as well as in Eqs. (3) and (5). More research is indeed needed to separately characterize these circumstances and to quantify their potential impact on field and laboratory liquefaction studies and $s_u(\text{yield})$.

6. Application to liquefaction analysis of sloping grounds

In order to account for the effect of soil dilatancy, Eq. (5) can be employed to calculate $s_u(\text{yield})/\sigma'_{vo}$ from a measured value of $s_u(\text{liq})/\sigma'_{vo}$.$s_u(\text{liq})$ can be directly measured by laboratory shear testing of undisturbed field samples obtained by ground freezing techniques (Hofmann et al., 2000) or by high-quality tube sampling and correcting $s_u(\text{liq})$ for the effects of changes in void ratio due to sampling, handling, and the test setup (Poulos et al., 1985). However, because of the inherent variability of the in-situ void ratio within a certain cohesionless soil layer, and the high sensitivity of $s_u(\text{liq})$ in cohesionless soils to void ratio variations and sample disturbance, a limited number of frozen soil samples and laboratory shear tests would not represent the in-situ $s_u(\text{liq})$ of the entire soil layer, particularly when significant stratification is present. Accordingly, SPT- and CPT-based empirical correlations (Idriss and Boulanger, 2007; Mesri, 2007; Olson and Stark, 2002; Robertson, 2010) are recommended to obtain the in-situ $s_u(\text{liq})/\sigma'_{vo}$. In particular, an electronic CPT detects thin liquefiable layers and rapidly provides a continuous profile of the soil variability with excellent repeatability and accuracy at lower costs than any other in-situ tests. Therefore, empirical correlations of CPT with $s_u(\text{liq})$ are more reliable and exhibit less scatter than those for $s_u(\text{yield})$. The SPT- and CPT-based

empirical relationships developed by Olson and Stark (2002) are considered more appropriate as they incorporate the effects of failure kinetics, potential hydroplaning, soil mixing, and the shear strength of non-liquefied soils in providing the best estimate of $s_u(\text{liq})/\sigma'_{vo}$. The aforementioned procedure is demonstrated in the following paragraphs for assessing the triggering of liquefaction for a dyke to the north of Wachusett Dam and Duncan Dam.

6.1. Dyke to the north of Wachusett Dam

Wachusett Dam is the main water supply reservoir for the city of Boston which is located about 48 km west of the city. On April 11th, 1907, the upstream shell of an adjacent dyke constructed of an uncompacted sand to silty sand deposit ($D_{50} \approx 0.42$ mm, FC=5–10%) at the north of Wachusett Dam underwent static liquefaction flow failure during the initial filling of its reservoir. Standard penetration tests carried out in the upstream fill soils indicated an average SPT blow count, $(N_1)_{60}$ of 7 (Olson et al., 2000), which corresponds to an average $s_u(\text{liq})/\sigma'_{vo}=0.083$ based on the empirical relationship of Olson and Stark (2002). Accordingly, an average liquefaction triggering $s_u(\text{yield})/\sigma'_{vo}=0.25$ is calculated from Eq. (5) for the loose upstream fill. This is slightly less than the initial driving shear stress ratio of 0.26–0.30 in the upstream slope of the dyke (Olson et al., 2000), and therefore, explains the occurrence of static liquefaction failure of the dyke. The resulting average $I_B=0.68$ (from Eq. (1)) is also within the range of those observed in the static liquefaction flow failures of Table 2.

6.2. Duncan Dam

Duncan Dam is located on the Duncan River about 8 km upstream of Kootenay Lake in British Columbia, Canada. The 39-m high dam consists of a zoned earth-fill embankment with a crest length of 792 m, which was founded on an approximately 380-m-thick deposit of liquefiable fine silty sand (Byrne et al., 1994). Although Duncan Dam has never experienced any liquefaction failures, the wealth of available data makes this an ideal case for evaluating Eqs. (3) and (5) in a liquefaction-triggering analysis. Normalized SPT blow counts, $(N_1)_{60}$ of 10 to 18 were measured in the loose sand beneath Duncan Dam (Plewes et al., 1994). These correspond to an average $s_u(\text{liq})/\sigma'_{vo}=0.135$ (ranging from 0.105 to 0.165) from the SPT-based empirical correlation of Olson and Stark (2002), and hence, average $I_B=0.481$ and $s_u(\text{yield})/\sigma'_{vo}=0.260$ from Eqs. (3) and (5), respectively. The calculated $s_u(\text{yield})/\sigma'_{vo}$ is within the range of $s_u(\text{yield})/\sigma'_{vo}$=0.23–0.28 measured in DSS tests on undisturbed specimens of Duncan Dam sand obtained by the coring of frozen samples (Pillai and Salgado, 1994).

From the limit equilibrium stability analysis of the original pre-failure geometry of Duncan Dam, Olson (2006) calculated an average driving shear stress ratio (τ_c/σ'_{vo}) of about 0.12. Liquefaction is triggered when the $s_u(\text{yield})$ calculated from Eq. (5) is exceeded by the total driving shear stress (including τ_c). Therefore, considering the relatively large increment of 0.14 (from $\tau_c/\sigma'_{vo}=0.12$) required to exceed $s_u(\text{yield})/\sigma'_{vo}=0.260$ and trigger liquefaction, as well as the relatively small $I_B=0.481$ of Duncan Dam, compared to those in the static liquefaction flow failures of Table 2, the risk of static liquefaction triggering and the occurrence of a catastrophic flow failure is comparatively remote for Duncan Dam. This corroborates with BC Hydro's report about the performance and liquefaction safety of this dam (Olson, 2006).

Accordingly, Eqs. (3) and (5) provide reasonable estimates of $s_u(\text{yield})/\sigma'_{vo}$ for the liquefaction-triggering analysis. Fig. 6 compares the estimates of Eq. (5) with those of Olson and Stark (2003). According to this figure, the key advantage

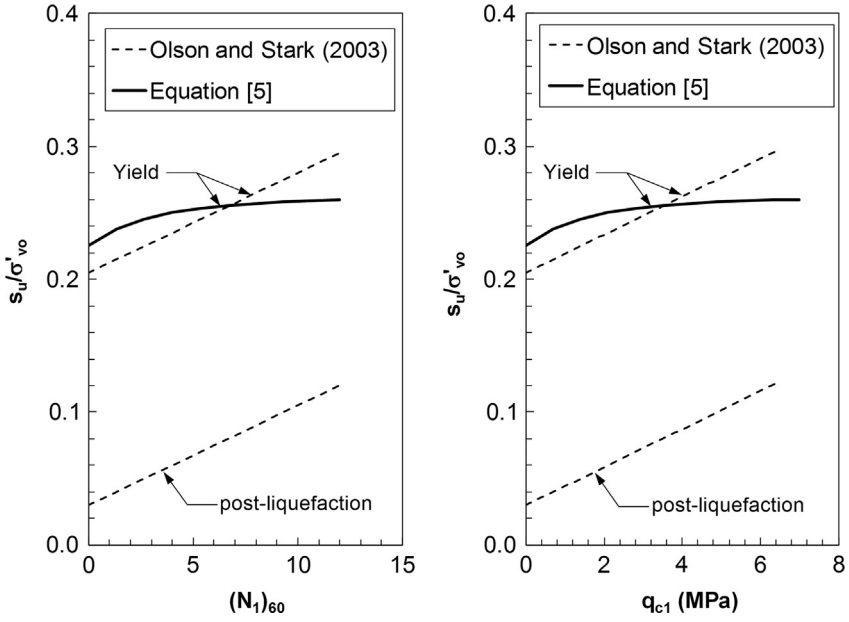

Fig. 6. Comparisons of $s_u(\text{yield})/\sigma'_{vo}$ relationships with (a) $(N_1)_{60}$, and (b) q_{c1} of Olson and Stark (2003) with those from Eq. (5).

of the proposed method is that the fundamental effect of the increasing soil dilatancy with the increasing penetration resistance (or D_{rc} in Fig. 2) on reducing the amount of undrained strength loss from s_u(yield) to s_u(liq) in cohesionless soils is accounted for in the estimation of s_u(yield), and hence, for the field liquefaction-triggering analysis. As the amount of kinetic energy imparted on a sliding soil mass depends on the amount of shear strength reduction upon failure, and thus, I_B (Bishop, 1973), the proposed method provides a potential mechanism for differences in the amount of travel distances among liquefaction flow failures, which is not possible with the existing empirical correlations presented in Fig. 3. For example, besides the possible effects of ground topography, boundary conditions, and hydroplaning, the larger I_B (see Table 2) associated with the liquefaction flowslide of the Merriespruit tailings dam ($I_B=0.89$; actual travel distance of 2000 m) would suggest a greater travel distance than that following the flow failure of Calaveras Dam ($I_B=0.58$; actual travel distance of about 200 m). Accordingly, Eq. (5) and the proposed technique implicitly provide vital information about the performance level of a sloping ground if liquefaction occurs. Besides, as Fig. 4 and Eqs. (3) and (5) are based on data from multiple modes of shear (DSS, HCTS, PSC, RS, and TxC), soil fabrics (moist tamped, air pluviated, water pluviated), and consolidation stress states (K_c=0.33–1.0 in the laboratory tests of Table 1), this procedure is applicable under all of these conditions.

Note that liquefaction also occurs under cyclic loads as a result of excess pore water pressure generation from a repeated number of loading and unloading shear stress cycles and the excursion of the effective stress path to the instability line without reaching s_u(yield), whereas exceeding s_u(yield) is the primary mechanism of static liquefaction by a monotonically-increasing triggering load in a saturated cohesionless soil. Therefore, the triggering mechanism of cyclic liquefaction events is quite different than liquefaction triggered by monotonically-increasing loads, and the approach proposed in this study is only applicable to liquefaction-triggering analyses of sloping grounds by monotonic loads. As a result of the failure to recognize this fundamental difference between monotonic and cyclic liquefaction triggering mechanisms, Olson and Stark (2003) and Olson (2001, 2006) erroneously extended the application of s_u(yield) to seismic liquefaction-triggering analyses. This would incorrectly assign much larger cyclic shear strengths to liquefiable soils or mark soil zones that would otherwise liquefy under a given cyclic load as non-liquefiable. Therefore, the application of their method to seismic liquefaction-triggering analyses could be excessively unsafe and is not recommended.

7. Conclusions

While the existing methods for liquefaction-triggering analyses of sloping ground conditions are either overly expensive or fail to account for the dilatancy behavior of cohesionless soils, an empirical approach has been developed in this study to estimate the liquefaction-triggering strength of strain-softening saturated cohesionless soils subject to a monotonically-increasing shear load. The proposed method accounts for the effect of increasing soil dilatancy – observed in a large database of laboratory experiments – with an increasing soil density or in-situ penetration resistance on reducing the amount of undrained strain-softening and brittleness of cohesionless soils. This allows the method to differentiate among liquefaction flow failures with different travel distances based on the amount of undrained strength reduction and brittleness exhibited following the initiation of liquefaction failure.

It has been demonstrated that the proposed method provides reliable estimates of the s_u(yield) mobilized in past liquefaction flow failures, which conforms to the fundamental physics of soil behavior by accounting for the effect of soil dilatancy.

Acknowledgments

The intellectual comments provided by the anonymous reviewers, which helped to improve the paper, are greatly appreciated.

References

Alarcon-Guzman, A., Leonards, G.A., Chameau, J.L., 1988. Undrained monotonic and cyclic strength of sands. J. Geotech. Eng. Div., ASCE 114, 1089–1109.

Andersen, K.H., Schjetne, K., 2012. Data base of friction angles of sand and consolidation characteristics of sand, silt, and clay. J. Geotech. Geoenviron. Eng., ASCE 139, 1140–1155.

Ayoubian, A., Robertson, P.K., 1998. Void ratio redistribution in undrained triaxial extension tests on Ottawa sand. Can. Geotech. J. 35, 351–359.

Batiste, S.N., Alshibli, K.A., Sture, S., Lankton, M.R., 2004. Shear band characterization of triaxial sand specimens using computer tomography. Geotech. Test. J., ASTM 27, 1–12.

Been, K., Jefferies, M.G., Hachey, J., 1991. The critical state of sands. Geotechnique 41, 365–381.

Bishop, A.W., 1971. Shear Strength Parameters for Undisturbed and Remoulded Soil Specimens., Roscoe Memorial Symposium. Cambridge University, Cambridge, Mass.3–58.

Bishop, A.W., 1973. The stability of tips and spoil heaps. Q. J. Eng. Geol. Hydrogeol. 6, 335–376.

Bjerrum, L., 1971. Subaqueous Slope Failures in Norwegian Fjords. Norwegian Geotechnical Institute, Oslo, Norway.

Bolton, M.D., 1986. The strength and dilatancy of sands. Geotechnique 36, 65–78.

Boulanger, R.W., Truman, S.P., 1996. Void redistribution in sand under post-earthquake loading. Can. Geotech. J. 33, 829–834.

Buscarnera, G., Whittle, A., 2013. Model prediction of static liquefaction: influence of the initial state on potential instabilities. J. Geotech. Geoenviron. Eng., ASCE, 139; 420–432.

Byrne, P.M., Imrie, A.S., Morgenstern, N.R., 1994. Results and implications of seismic performance studies for Duncan Dam. Can. Geotech. J. 31, 979–988.

Castro, G., 1969. Liquefaction of Sands. Harvard University, Cambridge, Massachusetts.

Castro, G., Enos, J.L., France, J.W., Poulos, S.J., 1982. Liquefaction Induced by Cyclic Loading. Report to National Science Foundation, Washington, D.C.

Chen, H.W., 1984. Stress–strain and Volume Change Characteristics of Tailings Materials. University of Arizona, Tucson, Arizona.

Chu, J., 1995. An experimental examination of the critical state and other similar concepts for granular soils. Can. Geotech. J. 32, 1065–1075.

Chu, J., Wanatowski, D., 2009. Effect of loading mode on strain softening and instability behavior of sand in plane-strain tests. J. Geotech. Geoenvirion. Eng., ASCE 135, 108–120.
Cubrinovski, M., Ishihara, K., 1999. Empirical correlation between SPT N-value and relative density for sandy soils. Soils Found 39, 61–71.
Davis, A.P., Poulos, S.J., Castro, G., 1988. Strengths backfigured from liquefaction case histories. In: Proceedings of the 2nd International Conference on Case Histories in Geotechnical Engineering, St. Louis, MO, pp. 1693–1701.
Dawson, R.F., Morgenstern, N.R., Stokes, A.W., 1998. Liquefaction flowslides in Rocky Mountain coal mine waste dumps. Can. Geotech. J. 35, 328–343.
DeGregorio, V.B., 1990. Loading systems, sample preparation, and liquefaction. J. Geotech. Eng., ASCE 116, 805–821.
Dennis, N.D., 1988. Influence of specimen preparation techniques and testing procedures on undrained steady state shear strength. In: Donaghe, R.T., Chaney, R.C., Silver, M.L. (Eds.), Advanced Triaxial Testing of Soil and Rock, ASTM STP 977. American Society for Testing and Materials, Philadelphia, pp. 642–654.
Di Prisco, C., Matiotti, R., Nova, R., 1995. Theoretical investigation of the undrained stability of shallow submerged slopes. Geotechnique 45, 479–496.
Doanh, T., Ibraim, E., Matiotti, R., 1997. Undrained instability of very loose Hostun sand in triaxial compression and extension. Part 1: experimental observations. Mech. Cohes.-Frict. Mater. 2, 47–70.
Finge, Z., Doanh, T., Dubujet, P., 2006. Undrained anisotropy of Hostun RF loose sand: new experimental investigations. Can. Geotech. J. 43, 1195–1212.
Fourie, A.B., Blight, G.E., Papageorgiou, G., 2001. Static liquefaction as a possible explanation for the Merriespruit tailings dam failure. Can. Geotech. J. 38, 707–719.
Fourie, A.B., Tshabalala, L., 2005. Initiation of static liquefaction and the role of K-0 consolidation. Can. Geotech. J. 42, 892–906.
Fuentes, W., Triantafyllidis, T., Lizcano, A., 2012. Hypoplastic model for sands with loading surface. Acta Geotech. 7, 177–192.
Gajo, A., Piffer, L., 1999. The effects of preloading history on the undrained behavior of saturated loose sand. Soils Found. 39, 43–54.
Gilbert, P.A., Marcuson, W.F., 1988. Density variation in specimens subjected to cyclic and monotonic loads. J. Geotech. Eng. Div., ASCE 114, 1–20.
Harris, W.W., 1994. Localization of Loose Granular Soils and its Effect on Undrained Steady State Strength. Northwestern University, Evanston, Illinois.
Hazen, A., 1918. A study of the slip in the Calaveras Dam. Eng. News Rec. 81, 1158–1164.
Highter, W.H., Tobin, R.F., 1980. Flow slides and the undrained brittleness index of some mine tailings. Eng. Geol. 16, 71–82.
Hird, C.C., Hassona, F.A.K., 1990. Some factors affecting the liquefaction and flow of saturated sands in laboratory tests. Eng. Geol. 28, 149–170.
Høeg, K., Dyvik, R., Sandbaekken, G., 2000. Strength of undisturbed versus reconstituted silt and silty sand specimens. J. Geotech. Geoenviron. 126, 606–617.
Hofmann, B.A., Sego, D.C., Robertson, P.K., 2000. In situ ground freezing to obtain undisturbed samples of loose sand. J. Geotech. Geoenviron. 126, 979–989.
Huang, Y.-T., Huang, A.-B., Kuo, Y.-C., Tsai, M.-D., 2004. A laboratory study on the undrained strength of a silty sand from Central Western Taiwan. Soil Dyn. Earthq. Eng. 24, 733–743.
Idriss, I.M., Boulanger, R.W., 2007. SPT- and CPT-based relationships for residual shear strength of liquefied soils. In: Pitilakis, K.D. (Ed.), 4th International Conference on Earthquake Geotechnical Engineering. Springer, Thessaloniki, Greece, pp. 1–22.
Ishihara, K., 1993. Liquefaction and flow failure during earthquakes. Geotechnique 43, 351–415.
Ishihara, K., Yasuda, S., Yoshida, Y., 1990. Liquefaction-induced flow failure of embankments and residual strength of silty sands. Soils Found. 30, 69–80.
Jamiolkowski, M., Ladd, C.C., Germaine, J.T., Lancelotta, R., 1985. New developments in field and laboratory testing of soils, Proceedings of the 11th International Conference on Soil Mechanics and Foundation Engineering. A.A. Balkema, San Fransisco, CA57–153.
Jefferies, M.G., 1993. Nor-Sand – a simple critical state model for sand. Geotechnique 43, 91–103.
Jefferies, M.G., Been, K., 2006. Soil Liquefaction – A Critical State Approach. Taylor & Francis, New York.
Kato, S., Ishihara, K., Towhata, I., 2001. Undrained shear characteristics of saturated sand under anisotropic consolidation. Soils Found. 41, 1–11.
Keyhani, R., Haeri, S.M., 2013. Evaluation of the effect of anisotropic consolidation and principle stress rotation on undrained behavior of silty sands. Sci. Iran. A 20, 1637–1653.
Kokusho, T., Kojima, T., 2002. Mechanism for postliquefaction water film generation in layered sand. J. Geotech. Geoenviron. 128, 129–137.
Konrad, J.M., 1993. Undrained response of loosely compacted sands during monotonic and cyclic compression. Geotechnique 43, 69–90.
Konrad, J.M., Pouliot, N., 1997. Ultimate state of reconstituted and intact samples of deltaic sand. Can. Geotech. J. 34, 737–748.
Koppejan, A.W., van Wamelen, B.M., Weinberg, L.J.H., 1948. Coastal landslides in the Dutch province of Zeeland. Second International Conference on Soil Mechanics and Foundation Engineering, 89–96 (Rotterdam, Holland).
Kramer, S.L., Seed, B.H., 1988. Initiation of static liquefaction under static loading conditions. J. Geotech. Eng., ASCE, 114; 412–430.
Kulasingam, R., Malvick, E.J., Boulanger, R.W., Kutter, B.L., 2004. Strength loss and localization of silt interlayers in slopes of liquefied sand. J. Geotech. Geoenviron. 130, 1192–1202.
Kulhawy, F.H., Mayne, P.H., 1990. Manual on Estimating Soil Properties for Foundation Design. Electric Power Research Institute (EPRI), Palo Alto, California2–38.
Lade, P.V., 1992. Static instability and liquefaction of loose fine sandy slopes. J. Geotech. Eng., ASCE 118, 51–71.
Lavigne, T.A., 1988. The Effects of Anisotropic Consolidation on the Liquefaction Potential of Mine Tailings. Department of Civil and Environmental Engineering, Clarkson University, Potsdam, New York.
Lee, K., L., 1965. Triaxial Compressive Strength of Saturated Sand Under Seismic Loading Conditions. University of California, Berkeley.
Malvick, E.J., Kutter, B.L., Boulanger, R.W., 2008. Postshaking shear strain localization in a centrifuge model of a saturated sand slope. J. Geotech. Geoenviron. 134, 164–174.
Mesri, G., 2007. Yield strength and critical strength of liquefiable sands in sloping ground. Geotechnique 57, 309–311.
Mizanur, R., Lo, S., 2012. Predicting the onset of static liquefaction of loose sand with fines. J. Geotech. Geoenviron. Eng., ASCE 138, 1037–1041.
Mooney, M., 1996. An experimental Study of Strain Localization and the Mechanical Behavior of Sand. Northwestern University, Evanston, Illinois.
Morrison, K.I., 1984. Case History of Very Large Submarine Landslide. In: Proceedings of the IV International Symposium on Landslides, Kitimat, British Columbia. pp. 337–342.
Mroz, Z., Boukpeti, N., Drescher, A., 2003. Constitutive model for static liquefaction. Int. J. Geomech., ASCE 3, 133–144.
Muhammad, K., 2012. Case history-based analysis of liquefaction in sloping ground. Department of Civil and Environmental Engineering, University of Illinois, Urbana, 489.
Mulilis, J.P., Arulanandan, K., Mitchell, J.K., Chan, C.K., Seed, H.B., 1977. Effects of sample preparation on sand liquefaction. J. Geotech. Eng. Div., ASCE 103, 91–108.
Murthy, T.G., Loukidis, D., Carraro, J.A.H., Prezzi, M., Salgado, R., 2007. Undrained monotonic response of clean and silty sands. Geotechnique 57, 273–288.
Olson, S.M., 2001. Liquefaction Analysis of Level and Sloping Ground Using Field Case Histories and Penetration Resistance. Department of Civil and Environmental Engineering, University of Illinois, Urbana, Illinois, 549.
Olson, S.M., 2006. Liquefaction analysis of Duncan Dam using strength ratios. Can. Geotech. J. 43, 484–499.
Olson, S.M., Stark, T.D., 2002. Liquefied strength ratio from liquefaction flow failure case histories. Can. Geotech. J. 39, 629–647.
Olson, S.M., Stark, T.D., 2003. Yield strength ratio and liquefaction analysis of slopes and embankments. J. Geotech. Geoenviron. Eng., ASCE 129, 727–737.

Olson, S.M., Stark, T.D., Walton, W.H., Castro, G., 2000. 1907 static liquefaction flow failure of the North Dike of Wachusett Dam. J. Geotech. Geoenviron. 126, 1184–1193.

Omar, T., 2013. Specimen Size Effect on Shear Behavior of Loose Sand in Triaxial Testing. Department of Civil and Environmental Engineering, Western University, London.

Park, S.-S., Byrne, P.M., 2004. Practical constitutive model for soil liquefaction. In: Pande, G.N., Pietruszczak, S. (Eds.), Numerical Models in Geomechanics (NUMOG IX). A. A. Balkema, pp. 181–187.

Pillai, V.S., Salgado, F.M., 1994. Post-liquefaction stability and deformation analysis of Duncan Dam. Can. Geotech. J. 31, 967–978.

Plewes, H.D., Pillai, V.S., Morgan, M.R., Kilpatrick, B.L., 1994. In-situ sampling, density measurements, and testing of foundation soils at Duncan dam. Can. Geotech. J. 31, 927–938.

Poulos, S.J., Castro, G., France, J.W., 1985. Liquefaction evaluation procedure. J. Geotech. Eng., ASCE, 111; 772–792.

Riemer, M.F., 1992. The Effects of Testing Conditions on the Constitutive Behavior of Loose, Saturated Sand Under Monotonic Loading. Department of Civil and Environmental Engineering, University of California, Berkeley, California.

Robertson, P.K., 2010. Evaluation of flow liquefaction and liquefied strength using the cone penetration test. J. Geotech. Geoenviron. 136, 842–853.

Sadrekarimi, A., 2009. Development of a New Ring Shear Apparatus for Investigating the Critical State of Sands. Department of Civil and Environmental Engineering, University of Illinois, Urbana-Champaign, Urbana, Illinois.

Sadrekarimi, A., 2013. Influence of state and compressibility on liquefied strength of sands. Can. Geotech. J. 50, 1067–1076.

Sadrekarimi, A., Olson, S.M., 2010a. Particle damage observed in ring shear tests on sands. Can. Geotech. J. 47, 497–515.

Sadrekarimi, A., Olson, S.M., 2010b. Shear band formation observed in ring shear tests on sandy soils. J. Geotech. Geoenviron. 136, 366–375.

Sadrekarimi, A., Olson, S.M., 2011. Critical state friction angle of sands. Geotechnique 61, 771–783.

Sasitharan, S., 1994. Collapse Behavior of Very Loose Sand. Department of Civil Engineering, University of Alberta, Edmonton.

Sassa, K., 2000. Mechanism of flows in granular soils, Proceedings of the International Conference on Geotechnical and Geological Engineering (GeoEng 2000). Technomic Publishing Company, Inc., Melbourne, Australia1671–1702.

Seid-Karbasi, M., Byrne, P.M., 2007. Seismic liquefaction, lateral spreading, and flow slides: a numerical investigation into void redistribution. Can. Geotech. J. 44, 873–890.

Sivathayalan, S., Ha, D., 2011. Effect of static shear stress on the cyclic resistance of sands in simple shear loading. Can. Geotech. J. 48, 1471–1484.

Sivathayalan, S., Vaid, Y.P., 2002. Influence of generalized initial state and principal stress rotation on the undrained response of sands. Can. Geotech. J. 39, 63–76.

Skirrow, R.K., 1996. The Effects of Fines Content on the Monotonic Triaxial Testing of Cohesionless Soils for Evaluation of In-situ State. Department of Civil Engineering, University of Alberta, Edmonton.

Sladen, J.A., D'Hollander, R.D., Krahn, J., 1985. The liquefaction of sands, a collapse surface approach. Can. Geotech. J. 22, 564–578.

Sladen, J.A., Handford, G., 1987. A potential systematic error in laboratory testing of very loose sands. Can. Geotech. J. 24, 462–466.

Spencer, E., 1967. A method of analysis of the stability of embankments assuming parallel interslice forces. Geotechnique 17, 11–26.

Stark, T.D., Mesri, G., 1992. Undrained shear strength of liquefied sands for stability analysis. J. Geotech. Eng., ASCE 118, 1727–1747.

Takeshita, S., Takeishi, M., Tamada, K., 1995. Static liquefaction of sands and its liquefaction index. In: Ishihara, K. (Ed.), Proceedings of the 1st International Conference on Earthquake Geotechnical Engineering. A.A. Balkema, Rotterdam, The Netherlands, Tokyo, Japan, pp. 177–182.

Terzaghi, K., Peck, R.B., Mesri, G., 1996. Soil Mechanics in Engineering Practice, Third Edition Wiley, New York.

Tsomokos, A., Georgiannou, V.N., 2010. Effect of grain shape and angularity on the undrained response of fine sands. Can. Geotech. J. 47, 539–551.

Vaid, Y.P., Eliadorani, A., 1998. Instability and liquefaction of granular soils under undrained and partially drained states. Can. Geotech. J. 35, 1053–1062.

Vaid, Y.P., Stedman, J.D., Sivathayalan, S., 2001. Confining stress and static shear effects in cyclic liquefaction. Can. Geotech. J. 38, 580–591.

Verdugo, R., 1992. Characterization of Sandy Soil Behavior Under Large Deformation. Department of Civil Engineering, University of Tokyo, Tokyo, Japan.

Wanatowski, D., 2007. Undrained instability of loose sand under plane-strain conditions and its engineering application. Found. Civil Environ. Eng. 10, 131–141.

Wanatowski, D., Chu, J., 2007. Static liquefaction of sand in plane strain. Can. Geotech. J. 44, 299–313.

Wanatowski, D., Chu, J., Loke, W.L., 2010. Drained instability of sand in plane strain. Can. Geotech. J. 47, 400–412.

Wang, F., 1999a. An Experimental Study on Grain Crushing and Excess Pore Pressure Generation During Shearing of Sandy Soils: A Key Factor for Rapid Landslide Motion,. Department of Civil Engineering, Kyoto University, Kyoto.

Wang, G., 1999b. An Experimental Study on the Mechanism of Fluidized Landslide. Civil Engineering, Kyoto University, Kyoto.

Wang, J., 2005. The Stress–Strain and Strength Characteristics of Portaway Sand., School of Civil Engineering. The University of Nottingham, Nottingham, UK, 303.

Wride, C.E., Robertson, P.K., 1997a. Phase I and III data review report (Mildred Lake and J-pit sites, Syncrude Canada Ltd.), CANLEX Technical Report. University of Alberta, Edmonton.

Wride, C.E., Robertson, P.K., 1997b. Phase II data review report (Massey and Kidd sites Fraser River delta), CANLEX Technical Report. University of Alberta, Edmonton.

Yoshimine, M., 1996. Undrained Flow Deformation of Saturated Sand Under Monotonic Loading Conditions. Department of Civil Engineering, University of Tokyo, Tokyo.

Yoshimine, M., Ishihara, K., Vargas, W., 1998. Effects of principal stress direction and intermediate principal stress on undrained shear behavior of sand. Soils Found. 38, 179–188.

Yoshimine, M., Robertson, P.K., Wride, C.E., 1999. Undrained shear strength of clean sands to trigger flow liquefaction. Can. Geotech. J. 36, 891–906.